A Review and Case Study of 3D Imaging Modalities for Female Amniote Reproductive Anatomy

Emma Clear[*,†,1], Robyn A. Grant[*], Michael Carroll[‡] and Charlotte A. Brassey[*]

[*]Department of Natural Sciences, Manchester Metropolitan University, Chester St, Manchester M1 5GD, UK; [†]Williamson Park Zoo, Quernmore Road, Lancaster, Lancashire LA1 1UX, UK; [‡]Department of Life Sciences, Manchester Metropolitan University, Chester St, Manchester M1 5GD, UK

From the symposium "Morphology and evolution of female copulatory morphology in Amniotes" presented at the annual meeting of the Society for Integrative and Comparative Biology virtual annual meeting, January 3–February 28, 2022.

[1]E-mail: emma.clear@stu.mmu.ac.uk

Synopsis Recent advances in non-invasive imaging methods have revitalized the field of comparative anatomy, and repro-ductive anatomy has been no exception. The reproductive systems of female amniotes present specific challenges, namely their often internal "hidden" anatomy. Quantifying female reproductive systems is crucial to recognizing reproductive pathologies, monitoring menstrual cycles, and understanding copulatory mechanics. Here, we conduct a review of the application of non-invasive imaging techniques to female amniote reproductive anatomy. We introduce the commonly used imaging modalities of computed tomography (CT) and magnetic resonance imaging (MRI), highlighting their advantages and limitations when applied to female reproductive tissues, and make suggestions for future advances. We also include a case study of micro CT and MRI, along with their associated staining protocols, applied to cadavers of female adult stoats (*Mustela erminea*). In doing so, we will progress the discussion surrounding the imaging of female reproductive anatomy, whilst also impacting the fields of sexual selection research and comparative anatomy more broadly.

Introduction

Non-invasive imaging methods, such as computed tomography (CT), magnetic resonance imaging (MRI), and ultrasound imaging are routinely used in veterinary and medical fields (Kasban et al. 2015). They provide the ability to rapidly identify, isolate, and animate internal anatomical features in three-dimensions (Fredieu et al. 2015) and allow for an in-depth exploration of anatomical structures, without the destruction of tissue and specimens associated with physical dissections (Doost et al. 2020). Advances in speed, resolution, and image processing methods have increased the use of these imaging methods in research, particularly in the fields of comparative anatomy and evolutionary biology (Mitteroecker 2020). Historically, data extracted from such images may have been subject to qualitative anatomical descriptions or simple linear measurements (Bookstein 1978). More recently, 3D geometric morphometrics (Adams et al. 2004) and shape complexity tools (Arslan et al. 2021) have allowed for the multivariate quantitative analysis of volumetric imaging data. Non-invasive imaging techniques have been adopted across vertebrate and invertebrate groups (Lauridsen et al. 2011), and have illuminated previously unknown features of locomotor (Tsai et al. 2020), feeding (Ross et al. 2012), respiratory (Dayan and Besoluk 2011), and sensory (Racicot 2021) anatomy.

The field of comparative reproductive anatomy has also benefited from advances in medical imaging technology and provides a specific set of methodological challenges. Some hurdles are shared across male and female genital anatomy. The high proportion of soft tissue and relative sparsity of mineralized elements characterizing vertebrate genitals (Kelly 2016) can limit image contrast in those modalities based upon tissue density. In addition, clear, unambiguous, homologous

landmarks are often lacking from soft tissue reproductive structures, limiting the application of 3D morphometrics or shape analysis to this data (Orbach et al. 2020). However, with more recent methodological developments such as sliding and surface semi-landmarking (Bardua et al. 2019), fully-automated landmarking (auto 3D GM; Boyer et al. 2015), 3D harmonic analysis (SPHARM; Shen et al. 2009), and other outline-based approaches (Bookstein 1997), quantitative measurements become more feasible, but have yet to be applied to female vertebrate reproductive systems. Other challenges facing the 3D imaging of reproductive anatomy are more specific to female genitalia. Relative to homologous male structures, female *external* genitalia are typically much reduced in size (Weiss et al. 2012). Furthermore, in vertebrates, they often have internal cavities (the vaginal tract and the uterus), which may be subject to compression and shape change, making them challenging to isolate from surrounding tissues (Orbach et al. 2016). The relative dearth of comparative anatomical studies applying medical imaging methods to female genitalia may also reflect the historical perception of female genitalia being less variable than male intromittent organs, and therefore, receiving less scientific attention (Ah-king et al. 2014).

Here, we summarize the current state of the field with regards to imaging female genital structures and present a methodological case study of the reproductive anatomy of the adult female stoat (*Mustela erminea*), with which we explore the benefits and current limitations of CT, MRI, and associated staining protocols applied to this organ system. We conclude with our suggestions for future avenues of research and methodological improvements that may be brought to bear on this important field of study.

A review of imaging techniques

We chose to limit the scope of our review to female amniotes, encompassing only those species undertaking internal fertilization. It has been hypothesized that the evolution of genital morphology in these species is driven by the direct interaction between the sexes during copulation (Eberhard 2010). Therefore, analyses of female genitalia, both their morphological diversity and their interaction with males, will illuminate potential coevolution and its wider ranging implications within the context of sexual selection. We chose to focus the review on the two technologies most frequently applied to the challenge of virtual dissection, CT, and MRI, with additional imaging methodologies, including sonography, also discussed in some detail.

X-ray CT

CT is a non-destructive imaging technique in which a source and detector are used to map X-ray attenuation through an intervening sample. A suite of projections is acquired at multiple angles surrounding the sample and subsequently reconstructed into a volumetric slice-based tomographic dataset (Sutton et al. 2013). Originally developed in the 1970's as a clinical diagnostic tool (Hounsfield 1973), CT is now highly valued for non-invasive 3D imaging in multiple fields including veterinary practice (Garland et al. 2002), palaeontology (Butler et al. 2022), biomechanics (Beaupied et al. 2007), and comparative anatomy (Santana 2018).

CT technology has improved greatly since its advent, most notably in terms of increased resolution and decreased acquisition time (Cunningham et al. 2014). Originally, whole-body medical CT scanning used a step-and-shoot technique, in which the sample was slowly moved through the rotating gantry, pausing at intervals to allow a trans-axial image to be captured (Hsieh et al. 2006). However, the advent of helical (or spiral) CT facilitated the capture of continuous data as 3D volumes, reconstructed using specialized algorithms (Sutton et al. 2013). Such scanners allow for improved visualization of small anatomical structures due to the retrospective ability to select the reconstruction plane (Hsieh 2000).

The development of multi-slice CT (comprising 4–256 detector rows) has further decreased acquisition times and reduced radiation dosages (Goldman 2008), particularly benefitting *in vivo* studies (Valente et al. 2007). Historically, slice thickness has been considerably coarser than the spatial resolutions achievable in-plane. However, multi-slice helical scanning can now generate isotropic voxels of dimensions in the range 0.3–3 mm (Sutton et al. 2013) and typically takes ~20 min to complete (Kinoshita et al. 2019). Micro CT offers even higher resolution images (1–100s μm) compared to helical scanning, but scan times are longer in the order of 30 min to several hours. Micro CT uses a cone-beam X-ray source and detector whilst rotating the sample (typically) 360° (Boerckel et al. 2014), allowing for a higher degree of rotational accuracy and control of the geometric magnification through manipulation of the distance between the source and the stage (Sutton et al. 2013). Micro CT was rapidly established as an essential tool for evaluating bone microstructure (Feldkamp et al. 1989), and has since been applied to a variety of both *in vivo* (Arai et al. 2005) and *ex vivo* samples, including imaging of soft tissues (Mizutani and Suzuki 2012). Resulting volumetric data can be digitally segmented to produce 3D models for quantitative analysis of morphology, such as geometric morphometrics (Hedrick

et al. 2019) and finite element analysis (Brassey et al. 2018), to examine functional and evolutionary hypotheses (Davies et al. 2017).

Unlike the other imaging modalities considered here (including MRI and ultrasound), CT relies upon ionizing radiation and can, therefore, induce damage and cause detrimental effects to biological tissues (Golding and Shrimpton 2002). For *in vivo* imaging, preferred scan parameters must, therefore, reflect a compromise between effective radiation dose and image quality, as determined by spatial resolution, contrast, and signal-to-noise ratio (Yu et al. 2009). As a general rule, micro CT imposes particularly high levels of ionizing radiation, due to the often-large number of projections, long exposure times and high spatial resolutions (Willekens et al. 2010).

Resulting CT images reflect X-ray attenuation through a sample, which is itself primarily a function of sample density and elemental composition. For this reason, when scanning amniote tissue, image contrast is particularly high between bony and soft tissues (Campbell and Sophocleous 2014). Skeletal elements may be segmented from surrounding soft tissue with comparative ease (van Eijnatten et al. 2018), whilst exposing the subtle differences between soft tissue structures is more challenging (Pauwels et al. 2013). As such, chemical staining agents are routinely applied to improve contrast at soft tissue boundaries (Descamps et al. 2014). Iodine-based contrast agents are particularly versatile agents, which can be intravenously administered to live specimens or used as staining solutions in which to submerge fixed specimens. Diffusible iodine-based contrast enhanced CT (diceCT; Gignac et al. 2016) is a technique relying on diffusion of iodinated agents through biological tissue as the iodine binds to naturally present carbohydrates and lipids, which enhances radiopacity during scanning (Gignac and Kley 2014). Phosphotungstic acid (PTA) has also been applied as a CT contrast agent and similarly diffuses through tissue binding to collagen and other proteins (Metscher 2011). However, PTA is typically slower to penetrate tissue than iodine and is acidic in solution, which could potentially lead to detrimental chemical and structural changes in the tissue (Metscher 2009).

CT applications to female amniote reproductive anatomy

Whilst CT has been widely applied to the challenge of imaging female non-human amniotes, there are still relatively few publications focused on female reproductive anatomy. Historically, the bulk of this research has occurred in the context of veterinary care (Gumpenberger 2017), where it has been employed to visualize numerous female reproductive structures, particularly in the diagnosis of vaginal (Weissman et al. 2013; Barozzi et al. 2021) and uterine lesions (Wenzslow et al. 2009; Hayashi et al. 2013), and ovarian tumors (Sontas et al. 2011; Pecile et al. 2017; Rowan et al. 2017), with much of this research conducted on domestic mammals. In birds, CT is the preferred tool for diagnosis of reproductive tract pathologies (Konicek et al. 2020), particularly ovarian cancers (Gillenwater 2017). CT has also been used to image ovarian follicles in reptiles, identifying the presence, size, and shape of eggs (Gumpenberger and Henninger 2001) and to determine sex in reptilian species with low levels of sexual dimorphism (Di Ianni et al. 2015).

In contrast, the application of CT to answer evolutionary questions beyond the scope of veterinary science is still limited in the context of female reproductive anatomy. CT data has, for example, identified the presence of complex vaginal folds in cetacean genitalia, which may act as a physical barrier to obscure suboptimal sperm and provide evidence of antagonistic coevolution (Orbach et al. 2017a), this contrasts with the body of research focused on the evolution of invertebrate genitalia (Wojcieszek et al. 2012; Sloan and Simmons 2019). As a result of concerted digitization projects (see oVert (2017)), there is a growing wealth of whole-body CT datasets available on digital platforms such as Morphosource (morphosource.org), many of which feature reproductive anatomy and could be used to explore clutch sizes or stages of reproductive development (Callahan et al. 2021). As the CT digitization of taxonomically diverse museum collections continues, the scope for addressing the evolution of female genitalia across interspecific datasets will further expand.

The majority of studies, herein, use medical helical CT of slice thicknesses between 1 and 5 mm, enabling scanning of the whole cadaver, retaining reproductive organ placement *in situ* and minimizing disruption of internal morphology (Samii et al. 2004; Wang et al. 2006; Valente et al. 2007; Cushing et al. 2013; Weissman et al. 2013; Agut et al. 2016; Veladiano et al. 2016; Gumpenberger 2017; Adkesson 2018; Barozzi et al. 2021). However, there are challenges in distinguishing reproductive structures in helical CT due to resolution and anatomical crowding of the pelvic region (Valente et al. 2007, Barozzi et al. 2021). For example, Veladiano et al. (2016) imaged three psittacine bird species and successfully resolved both the cloaca and ovaries, but not the oviduct, despite the use of an iodinated contrast agent. Helical CT can successfully facilitate the scanning of excised genitalia from much larger specimens, such as cetaceans (Orbach et al. 2017b).

In contrast, micro CT is typically applied to smaller samples (either small intact specimens, or excised tissues) and is capable of achieving higher resolutions. Nonetheless several challenges remain in applying mi-

cro CT to female reproductive anatomy, not least the mounting of soft tissues prior to scanning. Unlike helical CT (in which the specimen lies recumbent on the gantry) optimal mounting of samples for micro CT favors alignment of the specimen's long axis in the vertical direction (Sutton et al. 2013). Therefore, mounting specimens for micro CT often requires placing the specimen in low-density materials (cardboard, florist foam, and plastic tubing) and maintaining humidity to prevent desiccation and shrinkage during long scan times (du Plessis et al. 2017). However, excised soft tissues (such as genitalia) are prone to movement under the effect of gravity, leading to blurring of the images (Schambach et al. 2010). Wrapping specimens in soaked gauze (typically water, saline, ethanol, formalin, or isopropanol) provides moisture and some stability, but still carries the risk of tissue slumping, especially for thin or fragile structures such as the reproductive tract. Perhaps for this reason, micro CT is still rarely applied to female reproductive tissues. It has provided some insight into genital characteristics of extremely small vertebrate species (chameleons; Glaw et al. 2021) and in imaging embryonic cloaca (Tschopp et al. 2014), but is unlikely to have reached its full potential as an imaging modality.

Many studies use an iodine contrasting agent, most commonly administered intravenously to live animals (Samii et al. 2004; Wang et al. 2006; Wenzlow et al. 2009; Hayashi et al. 2013; Weissman et al. 2013; Agut et al. 2016; Veladiano et al. 2016; Barozzi et al. 2021). Due to the complex internal structures present in female amniote reproductive anatomy a specialized contrast-enhancing procedure, hysterosalpingography (HSG), can alternatively be performed *in vivo* to specifically visualize the uterus and fallopian tubes. HSG involves a cannula inserted into the cervix, through which a (typically iodine-based) contrast agent is injected, highlighting the shape of the uterus and fallopian tubes during examination. This technique is not restricted to a single imaging modality and has been used with conventional X-ray radiography (Ramsay et al. 1985), CT (Abdelrahman et al. 2014), and MRI (Lee Jr et al. 1996) as a potential precursor to more invasive diagnostic procedures.

Of those studies conducting staining on cadaveric material, there is no standardization of the length of time necessary for iodine staining, since it varies with specimen size and depth (Pauwels et al. 2013; Gignac and Kley 2018). Orbach et al. (2017b) submerged the interacting genitalia of male and female cetaceans and pinnipeds for 2 weeks, successfully imaging surfaces of genital structures but achieving limited stain penetration into the deeper soft tissues, whilst Moore et al. (2021) following a similar workflow, stained the genitals of the American alligator (*Alligator mississippiensis)* for "several" weeks. Unsurprisingly, smaller specimens require less concentrated iodine solutions and shorter stain times (Gignac et al. 2016). In these cases, PTA staining may be considered as an alternative. However, it is less common in the surveyed literature, perhaps due to the inability of PTA to stain at depths beyond ~2 mm (Metscher 2011). PTA has, however, been used to enhance contrast during micro CT of embryonic amniote cloaca (Tschopp et al. 2014).

The progression from medical CT to micro CT, alongside the deployment of staining protocols, has enhanced our ability to resolve the often thin and membranous tissues of the female reproductive system. The increasing availability of lab-based micro CT capable of scanning specific *regions of interest* and achieving *sub-micron* resolutions will undoubtedly further impact upon the field. Our case study (below) presents micro CT data of female amniote reproductive anatomy generated on two systems capable of different resolution ranges (0.25–25 μm, and 5–125 μm) in order to explore the potential benefits of enhanced resolution applied to such tissues.

MRI

MRI is a common non-invasive pre-clinical and clinical imaging technology, primarily for soft tissues (Ziegler et al. 2011), potentially lending itself well to soft tissue reproductive anatomy visualization and measurement. The absence of ionizing radiation in MRI, compared to radiological techniques such as CT, is a benefit that allows for repeated scans during reproductive monitoring of individuals without the risk of extensive radiation exposure (Wiczyk et al. 1988). Unlike CT, which uses X-rays, MRI uses strong magnets (typically between 1.5 and 9.4 Tesla (T)) to force protons within the tissue to align with their magnetic field. The alignment is then perturbed when radio-frequency energy is pulsed through the tissue. When the energy is on, protons spin out of equilibrium and against the magnetic pull, and when turned off protons realign with the magnet and release electromagnetic energy. Unlike radiological imaging, in which contrast depends on X-ray attenuation of the structures, MRI contrast is a function of how quickly this energy is released in various tissues (Carr and Grey 2002). Different image types can be created by varying either the time of repetition (TR), the amount of time between successive pulses or the time of echo (TE), the time between the delivery of pulse and the echo signal. T1-weighted images are characterized by short TR and TE times, which display as bright contrast in images such as fatty tissue. Whereas T2 are

produced by long TR and TE times and display as bright contrast in both fatty tissue and water (Bitar et al. 2006).

MRI scan resolution depends upon several factors including specimen size, field of view, magnet strength, and gradient strength (Moser et al. 2009). Depending on the size of the specimen, differences in coil setup can also inf l uence f i nal image quality. Preclinical coils typically hold samples up to the size of a large rat, whilst smaller specimens scanned in the same coils will achieve a finer spatial resolution due to a nar-rower field of view (Allisy-Roberts and Williams 2007). Clinical scanners are intended for human use and usu-ally feature a magnet strength between 0.5 and 3 T. Such scanners can, however, be fitted with bespoke coils to visualize medium-sized animals that are oth-erwise too large for preclinical machines (Pinkernelle et al. 2008). However, ultra-strength preclinical scan-ners (such as a 9.4 T) provide overall better visualiza-tion of the inherently small structure size of reproduc-tive anatomy of many small animal models (Avni et al. 2015).

MRI protocols may also differ in how the data is collected, either as single slices or volumetrically (Ziegler and Mueller 2011). Single-slice MRI scans can be processed very quickly enabling high throughput at a high resolution, but risk bypassing discrete structures or tissue-types (Shen et al. 2012). Czisch et al. (2001) suc-cessfully obtained 2D slice data of bird ovarian follicles in scans of ∼5 min, with slice thickness of 0.5–1 mm and at a resolution of 150 μm, with the additional ad-vantage of the animals not requiring anaesthesia or re-covery time from the procedure. Volumetric imaging, on the other hand, collects data on many contiguous slices in one region but can take several hours to com-plete (Ziegler et al. 2011). Whilst modern MRI can gen-erate a volumetric tomographic stack, the potential for segmenting and quantifying the 3D geometry of the female reproductive system from such data has not been explored to the same extent as equivalent volumetric CT datasets, and our case study is the first to do this (see Results below).

Compared to CT, MRI can differentiate between soft-tissue structures at high voxel resolutions without the need for contrast enhancement (Sundaram and McLeod 1990). Indeed, some pathologies benefit from non-contrast enhanced MRI, particularly imaging of blood vessels (Edelman and Koktzoglou 2019) and kidneys (Mannelli et al. 2012). However, many MR images can be enhanced through gadolinium-based contrast agents, which predominantly perform better on T1-weighted scans (Ibrahim et al. 2018). Gadolinium is a non-toxic paramagnetic substance which, when absorbed into the tissue, enhances the relaxation of the neighboring water protons and increases the positive signal on a T1-weighted image (Xiao et al. 2016). It can be administered to live specimens orally, intravenously, or via inhalation. Cadaveric specimens can also be submerged in a gadolinium-staining solution following a similar workflow to that established by other imaging techniques (diceCT, PTA-staining; Kim et al. 2009). Whilst contrast agents are considered safe for most medical use, there are some concerns regarding adverse effects of gadolinium exposure on embryos (Bird et al. 2019), which is a clear concern when examining reproduction in live females.

MRI applications to amniote female reproductive anatomy

MRI examinations have been used extensively in a human clinical context since its first application in 1977 (Geva 2006) and applied to gynaecological problems such as Müllerian duct abnormalities (Behr et al. 2012), uterine myomas (Valentin 2006), and endometriosis (Kinkel et al. 2006). In contrast, the application of MRI to non-human amniote female reproductive anatomy is relatively uncommon but does span a range of amniote groups including primates (Du et al. 2010; Avni et al. 2015), other mammals (Flouri et al. 2021; Ypsilantis et al. 2021), reptiles (Straub and Jurina 2001), and birds (Czisch et al. 2001) and has identif ied a suite of female reproductive organs.

In rhesus macaques (*Macaca mulatta*), changes in uterine dimensions over the course of menstrual cycles were monitored with MRI, alongside visualization of the uterine horn and ovaries (Du et al. 2010). In this instance, presence and thickness of endometrial lining were also identified and measured based on MRI images. The reproductive anatomy of the laboratory rat has also been visualized and described through the early stages of pregnancy by MRI via the detection of uterine bulges and embryonic vesicles (Ypsilantis et al. 2021), with placentome development similarly characterized by MRI in the pregnant ewe (Flouri et al. 2021). Additionally, ovarian follicles and the presence of eggs have been imaged in the red-eared terrapin (*Trachemys scripta elegans*; Straub and Jurina 2001) and the garden warbler (*Sylvia borin*; Czisch et al. 2001) using MRI. Most of these studies take an exploratory approach, with the aim of evaluating the feasibility of MRI use as a method of reproductive monitoring. Few attempts have been made to quantify female reproductive anatomy using MRI, with extracted data being limited to 2D measurements of uterus length, width, and endometrial thickness.

Previous MRI imaging of the female reproductive tract has used both T1 and T2 weighted images. Du et al. (2010) distinguished the cervix and multiple layers of

the uterus primarily using T2-weighted imaging, noting changes in thickness of the endometrium throughout the menstrual cycle. Similarly, changes in signal intensity in T2-weighted images enabled identification of the size and number of eggs in ovarian follicles of both reptiles (Straub and Jurina 2001; Kummrow et al. 2010) and birds (Czisch et al. 2001). A technique known as Short T1 Inversion Recovery (STIR) has also been used to produce 3D MR images of the pregnant rat uterus. This technique acts to suppress signal for fat and instead highlight only water (Fleckenstein et al. 1991), enhancing reproductive structures that would normally be surrounded by adipose tissue (Ypsilantis et al. 2021).

The majority of these studies feature MRI of female reproductive anatomy in live animals (Czisch et al. 2001; Straub and Jurina 2001; Kummrow et al. 2010; Erlacher-Reid et al. 2013; Aymen et al. 2020; Ypsilantis et al. 2021), for medical research (Stolzenburg et al. 2006; McNanley et al. 2009), or as a diagnostic tool in veterinary medicine (Gavin 2011). Relative to *in vivo* imaging, *ex vivo* MRI can benefit from longer scan times and decreased subject motion, allowing for improved spatial resolutions and decreased signal-to-noise ratios (Shatil et al. 2016). MRI is, therefore, a promising method for imaging cadaveric specimens (Zarb et al. 2017) or fixed museum specimens (Berquist et al. 2012). Yet cadaveric MRI is not without challenges, as chemical fixatives are known to alter various MRI properties (Shatil et al. 2016). Moreover, samples must be mounted in a medium such as formalin, phosphate-buffered saline, or agarose gel during scanning to mitigate scan artefacts at the air-tissue boundary, and air bubbles must be excluded from the fluids (Shatil et al. 2016). Perhaps for these reasons, there is a scarcity of published work compared to studies using CT. While Danil et al. (2014) did apply both MRI and CT to a cadaveric dolphin, they conducted no measurements, and produced no reconstructions of the reproductive region. Our case study presented here is the first example of MRI data of the non-human female reproductive region collected from fixed cadaveric material, alongside segmentation and 3D reconstruction of morphology.

Additional techniques

Traditionally, histology and scanning electron microscopy have been used to image tissue of the female reproductive tract, including the ovaries (Palmer and Guillette Jr. 1988; Ziehmer et al. 2010), oviducts (Rumery and Eddy 1974; Perkins and Palmer 1996), uterus (Psychoyos and Mandon 1971), and vagina (Lamb et al. 1978; Mayor et al. 2013). Whilst such techniques can provide valuable information on the microscopic structure of biological tissues and associated pathologies, they also damage or destroy the specimen (Sutton et al. 2013) and provide little insight into the gross morphology and organ arrangement of the female tract.

Beyond "tomographic" slice-based imaging techniques such as CT and MRI, ultrasound, is also used to image the reproductive system of larger species, especially in the agricultural industry. Ultrasound, or sonography, has been used to advance our understanding of the ovarian cycle (Waberski et al. 1999; Lazaridis et al. 2012), pregnancy status (Garcia et al. 1999), and artificial insemination (Lemma 2013) of cattle (dairy farming). Ultrasound can provide anatomical information on soft-tissue and organs via differential transmission and reflection of ultrasonic sound waves in the frequency range of 3–5 MHz up to 30–50 MHz (Kagadis et al. 2010), creating a 2D grayscale image, whereby the amplitudes of returning ultrasound waves are depicted as a function of brightness (Wells 1999). Linear "digital calliper" measurements of anatomical structures can quickly be captured from ultrasound images (England and Allen 1989) during routine data collection from large herds. Ultrasound interpretation is typically conducted by experienced technicians and can be used in tandem with vaginal cytology and mucus scoring (Williams et al. 2005; Aungier et al. 2012) as a diagnostic precursor to CT or MRI (Verstraete and Lang 2000). Whilst ultrasound is typically performed on live animals, recent studies have successfully applied the technology to cadaveric material (Ali and Derar 2020; Wahid et al. 2020) to delineate reproductive structures and their dimensions.

Silicone casting is a technique that physically models the morphology of the female reproductive tract and has so far been demonstrated in cadaveric dogfish (*Squalus acanthias*; Hedrick et al. 2019), alpaca (*Vicugna pacos*; Brennan et al. 2021), and caiman (*Caiman latirostris*; Moore et al. 2021), as well as various species of pinnipeds and cetaceans (Orbach et al. 2017b). The method involves filling the vaginal cavity with liquid rubber, often dental-grade silicone, and carefully removing the endocast when cured. Digital 3D models of female internal endocasts can then be produced via surface-based laser scanning or photogrammetry, and subsequent measurement and shape analyses conducted (Tsuboi et al. 2020). The repeatability of casting is high (Orbach et al. 2017b), and variability in casting agents has been found to have little impact on resulting endocast geometry (Brennan et al. 2021). However, the degree to which endocasts reliably conform to internal contours remains somewhat unclear.

Case study

The preceding review has identified several non-invasive imaging technologies that have been previously applied to female amniote reproductive tissues. Some methodologies are well-established (CT, Ultrasound), whilst others are nascent within the field (MRI). The most appropriate imaging technique to deploy in any given instance is a function of both the material under investigation and the research question being addressed. Only limited studies have applied multiple imaging technologies to the same structures (see Gartrell et al. (2002); Du et al. (2010); Erlacher-Reid et al. (2013); Danil et al. (2014); d'Ovidio et al. (2015) as examples). There are few robust methods for quantifying the morphology of internal soft-tissue reproductive structures; therefore, it is a challenge to meaningfully compare image contrast or stain uptake across modalities and assess their suitability for imaging female reproductive systems.

Here, we present a short case study, applying a suite of modern imaging tools to visualize the female reproductive anatomy of adult stoats (*M. erminea*), and compare the practicality of use and image quality between techniques. Stoats were selected due to their frequent availability in museum and research collections and their body size (representing the upper extreme of pelvic widths a small-bore MRI can accommodate). We apply micro CT (Figs. 1 and 2), silicone casting (Fig. 3), and MRI (Fig. 4), alongside appropriate staining protocols to the reproductive soft-tissue structures in the female stoat. We bisected each specimen horizontally across the trunk of the body, removing all tissue located cranial to the kidneys. All specimens were fixed in 10% neutral buffered formalin, apart from the sample used for silicone casting, which was not fixed but prepared and imaged within 48 h after thawing. We conducted micro CT imaging on three specimens. One remained unstained and was scanned in a Nikon Metrology 320 kV Custom Bay (Nikon, Hertfordshire, UK). The second specimen was submerged in a buffered-Lugol's iodine solution (following Dawood et al. 2021, see supplementary material for formula and protocol), and after 3 weeks scanned using a Zeiss Versa 520 (Zeiss, Oberkochen, Germany). Following an additional 11 days of staining, the same specimen was subsequently scanned in a Nikon Metrology "High Flux" bay. We used a third specimen to produce endocasts of the lumen of the reproductive tract using Mold Star® 16 FAST dental silicone (Smooth-On, Easton, Pennsylvania, USA) This specimen was micro CT scanned with the silicone endocast inside the tract in the Nikon Metrology "High Flux" bay. MRI scanning was conducted using a 9.4 T Bruker Biospec 94/20 USR horizontal bore MRI scanner (Bruker, Coventry, UK) with a T1-weighting on two specimens, one of which was submerged in a gadolinium-based staining agent for 1 month. Image segmentation was conducted in Dragonfly (2021; version 2021.1) using a combination of automated gray-scale thresholding and manual segmentation. Several software packages exist for the segmentation and meshing of CT data (e.g., VG Studio Max, Avizo, and 3D Slicer), all with differing functionality, which may ultimately impact upon the segmentation masks and surface models generated. Here, we have restricted ourselves to Dragonfly's "global threshold" and basic region-of-interest paintbrush tools, which ought to be comparable across packages (see Supplementary Material for more detailed methods information).

Results

All scanning modalities resulted in unique image datasets, depending upon scan parameters and contrast stains used. Upon dissection, we noted that one specimen had larger reproductive anatomy (Fig. 1D) compared to the other four, featuring larger ovaries, oviducts, and uterine horn. Oviduct width (taken post-examination using our 3D models in the frontal plane) was linearly measured at multiple corresponding points and averaged at 1.85 and 2.32 mm for the "normal" specimens (Fig. 4C and 4F, respectively), but 3.5 mm in the anomaly, despite this animal's overall body size being considerably smaller. Based on observations of closely related species, whilst there was no evidence of embryos present, it is likely that this difference in size can be attributed to a recent pregnancy in this animal (Amstislavsky and Ternovskaya 2000; Lindeberg 2008). This seasonal change in anatomy is a potentially confounding issue to consider when imaging female reproductive anatomy. CT images of the unstained specimen (Nikon 320 kV bay) achieved a 30 μm resolution and took ~1 h to complete (Fig. 1B). As expected, images were characterized by good contrast between bone and soft tissue, successfully resolving the skeletal elements. However, very little contrast was achieved between soft tissue types. Gray-scale values extracted from a transect across the pelvis were found to peak at locations corresponding to bone, but otherwise remained relatively constant across the soft tissue (Fig. 1B, inset plot). Due to the contrast between mineralized and unmineralized tissues, 3D surface models of the skeleton could be automatically generated using threshold segmentation (Fig. 1C). The iodine-stained CT scan (Nikon High-Flux bay, 32 days in stain) was conducted at a resolution of 21 μm over the course of ~3 h (Fig. 1E). Resulting images showed a substantial increase in soft-tissue contrast;

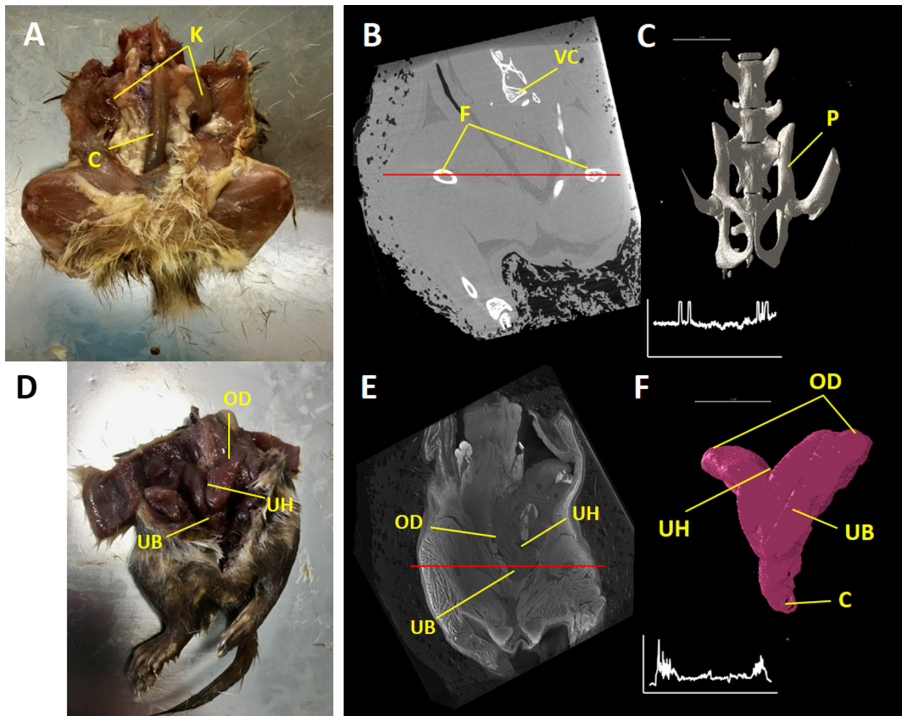

Fig. 1 (**A**) and (**D**) Female stoat specimens were bisected and the cavity opened to ensure optimal uptake of iodine solution, internal organization was preserved where possible. (**B**) Slice data taken of the coronal plane of the unstained specimen in micro CT—specimen displays very little soft tissue contrast, yet skeleton is easily resolvable. Transect line (red) runs between right femur and left femoral head. Plot (inset) identifies gray-scale values extract along transect using the PeakFinder tool (Vischer 2013). Peaks correspond to bone cortices. (**C**) 3D model of the pelvic region of the unstained specimen—reproductive tract could not be segmented. Scale bar representative of 10 mm. (**E**) Slice data taken of the coronal plane of the micro CT scan of the stained specimen—iodine stain improves muscle tissue contrast, and also highlights internal organs. Transect plot (inset) highlights "halo" effect on incomplete staining, but does identify smaller localized peaks internally. (**F**) 3D model of the female reproductive tract, from the uterus to uterine horn and branching oviducts, of the stained specimen—tract was discernible for manual segmentation. Iodine staining causes reduced contrast between bone and soft tissue, however, making skeletal segmentation a challenge. Scale bar representative of 10 mm. Figure key: C—colon; K—kidney; F—femur; VC—vertebral column; P—pelvis; OD—oviduct: UH—uterine horn; UB—uterine body; and C—cervix

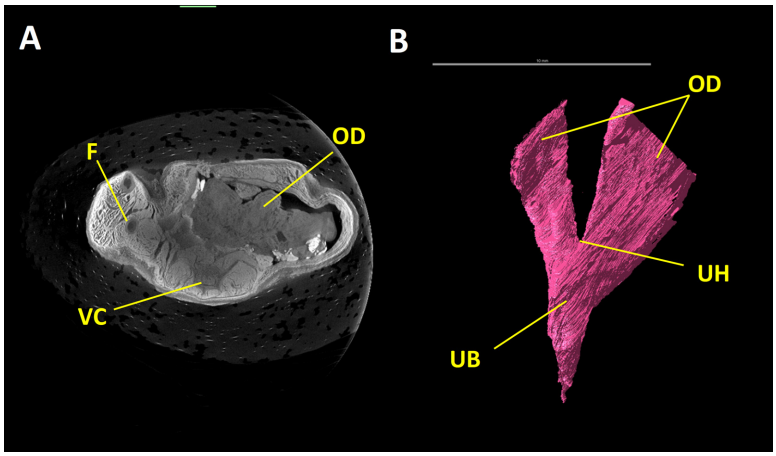

Fig. 2 (**A**) Slice data taken on the transverse plane of the stained specimen in micro CT (Zeiss Versa)—iodine-contrast agent has stained the external margins, and also provided improved contrast enhancement to the internal organs. (**B**) 3D model of the female reproductive tract, from the uterus to uterine horn and branching oviducts, taken from micro CT (Zeiss Versa) data of a stained specimen. Scale bar representative of 10 mm. Figure key: F—femur; VC—vertebral column; OD—oviduct; UH—uterine horn; and UB—uterine body

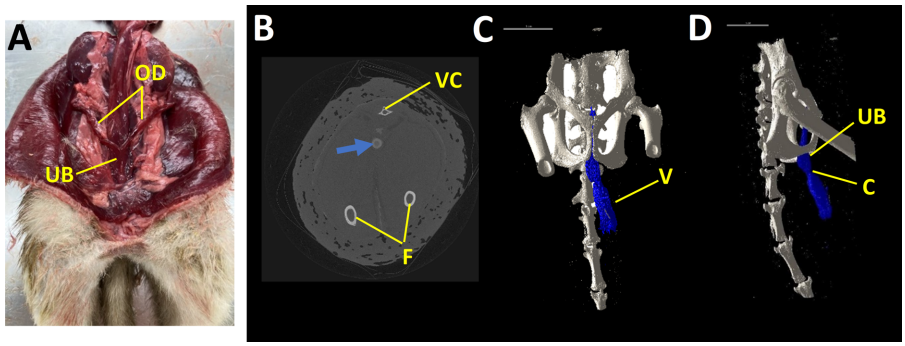

Fig. 3 (**A**) Female stoat specimen was bisected and opened, but internal organization was preserved where possible. (**B**) Slice data taken on the transverse plane of the unstained specimen in micro CT—blue arrow identifies the internal cavity and area filled with silicone rubber. (**C**) 3D model of the pelvic bone region and silicone cast *in situ* in the frontal plane. Scale bar representative of 10 mm. (**D**) 3D model of the pelvic bone region and silicone cast *in situ* in the sagittal plane. Scale bar representative of 10 mm. Figure key: OD—oviduct; UB—uterine body; VC—vertebral column; F—femur; V—vagina; and C—cervix

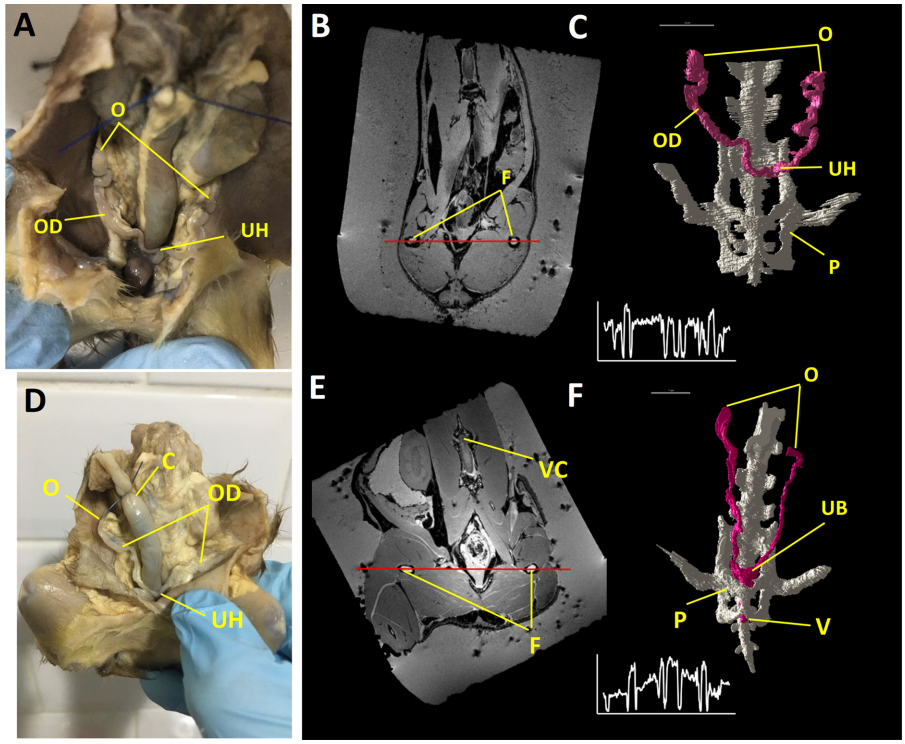

Fig. 4 (A) and (D) Female stoat specimens were bisected, and the cavity opened to ensure optimal uptake of gadolinium-based contrast agent, yet internal organization was preserved where possible. (B) Slice data taken on the coronal plane of the unstained specimen in MRI—specimen displays some soft tissue contrast. Transect line (red) runs between femurs. Plot (inset) identifies gray-scale values extracted along transect using the PeakFinder tool (Vischer 2013), with several peaks discernible inside the cavity. (C) 3D model of the pelvic region and the reproductive tract of the unstained specimen—ovaries and oviducts were visible for manual segmentation, but tract was not distinguishable below the uterine horn. Scale bar representative of 10 mm. (E) Slice data taken on the coronal plane of the MRI scan of the stained specimen—contrast agent has further illuminated internal architecture, muscle architecture, and bone. Transect plot (inset) displays a smoother variation between high and low gray-scale values. (F) 3D model of the female pelvic region and reproductive tract—ovaries, oviducts, uterus, and upper vagina were visible. Both reproductive tract and bones were manually segmented. Scale bar representative of 10 mm. Figure key: O—ovaries; OD—oviduct; UH—uterine horn; F—femur; P—pelvis; C—colon; VC—vertebral column; UB—uterine body; and V—vagina

the outer layers of tissue, those most in contact with the iodine stain, showed particularly strong contrast. The reproductive tract, including the uterus, oviducts, and ovaries, were identifiable and could be segmented manually, on a slice-by-slice basis (Fig. 1F). Gray-scale values extracted across a pelvic transect peaked at the

outer tissues and decreased internally (Fig. 1E plot), indicating incomplete staining of the specimen. However, smaller localized peaks internally indicate the presence of some soft tissue contrast that was not present in unstained sample.

Micro CT scanning using the Zeiss Versa 520 was conducted on the same stained specimen as used in the previous micro CT images after only 21 days in stain. Whilst this machine has the capacity to produce images at the sub-micron level, this was unachievable for the dimensions of our specimen. The images generated are of the highest resolution of all modalities considered here, however, at 17 μm and took ~12 h (Fig. 2A). The deep tissues clearly remain understained. A 3D reconstruction of the female reproductive tract could be manually segmented, however, including the branching oviducts, uterine horn, and uterine body (Fig. 2B), the vagina could not be resolved. Despite the comparatively short stain time relative to the High Flux bay, the Versa generated higher resolution images, and it, therefore, proved easier to manually segment internal reproductive anatomy.

A physical endocast of the vaginal lumen of the stoat was also created and micro CT scanned in an unstained specimen (Fig. 3A) over 37 min at a resolution of 25 μm. Due to the small size of the specimen, it was difficult to confirm how far the silicone had penetrated within the tract prior to scanning without risking damage to the internal tissue. However, the silicone was easily identifiable in CT slice data (Fig. 3B) and the endocast could be digitally segmented by hand. The 3D model (Fig. 3C and D) provides evidence that the silicone travelled through the vulva, into the vagina, cervix, and uterus.

Specimens used in the MRI protocol were more similarly sized and featured no obvious pathologies (Fig. 4A and D). Each MRI scan took ~4–6 h to complete, regardless of staining agent. In contrast to what was expected, the unstained MRI images had a better quality resolution than the stained, at 166 μm (Fig. 4B). This technique also provided better soft tissue contrast than that of unstained CT (see Fig. 1B), permitting identification and manual segmentation of the ovaries and oviducts and adjacent skeletal elements (Fig. 4C). Transects extracted across the unstained MRI scans showed a large variation in gray-scale values (Fig. 4B plot), illustrating better contrast between soft tissue types than CT, despite lower spatial resolution. There were, however, difficulties accurately identifying soft-tissue structures located between the uterine horn and the vulva, potentially due to the crowding within this pelvic area. The stained MRI scans had a 194 μm resolution and provided soft tissue contrast of consistent quality throughout the specimen (Fig. 4E). Transects across the stained MRI (Fig. 4E plot) illustrated good contrast between tissue types, similar to that of the unstained MRI data. However, the staining agent provided enhanced contrast in the region within the pelvis, facilitating the identification of the uterus and vagina (Fig. 4F).

Outstanding problems for imaging female genital anatomy

The advantages of imaging female reproductive systems are clear—from the non-invasive diagnostic imaging of veterinary case studies, to the creation of large-scale image databases for the purpose of comparative anatomy and functional morphology (Ziegler et al. 2010). Indeed, the development and sharing of digital images and data can give rise to large comparative datasets capable of addressing fundamental questions on comparative anatomy and evolution of species. The development of digital imaging modalities has enabled us to image features of female internal genital anatomy, including ovaries, oviducts, and the uterus at resolutions of 17 μm (micro CT) and 166 μm (MRI). Our case study highlights the capacity to successfully capture female reproductive morphology via multiple scanning techniques, particularly the use of staining agents in both CT and MRI applications. However, female reproductive anatomy still presents persistent challenges for 3D imaging, and all imaging techniques provide unique advantages and challenges to visualizing this organ system. These can include, but are in no way limited to, issues with image contrast, staining, resolution, scan times, and speed of segmentation.

Both MRI and CT can struggle with image contrast in the window of soft tissues (Wenzlow et al. 2009; Barozzi et al. 2021), and this was reflected in our own case study (Figs. 1B and 4B). Indeed, despite > 4 weeks staining, sample agitation, stain refresh, and considerable tissue surface area across which uptake could occur, our sample remained under-stained in some deeper regions of tissue. Phase-contrast CT may be a viable solution to this challenge. Phase-contrast CT relies upon X-ray diffraction, as opposed to X-ray attenuation, and shows strong potential in the imaging of low density and low-Z (atomic number) materials, such as biological specimens (Tao et al. 2021). Although typically still applied in the context of large synchrotron facilities, phase contrast has been successfully deployed on lab-based micro CT sources to image cadaveric mice thorax (Hagen et al. 2020) and resolve fiber orientation in the murine heart (Reichardt et al. 2020) but, as far as the authors are aware, has yet to be applied to reproductive tissues.

Staining protocols have also been developed to improve image contrast. However, for cadaveric studies, concentrations and timings can drastically differ be-

tween specimens and tissue types (Gignac et al. 2016) and it is, therefore, challenging to produce standardized protocols. Many CT staining studies are still conducted on a somewhat trial-and-error basis, proving costly both in terms of user and scan time. Some staining protocols may also damage specimens, ruling them unsuitable for more delicate structures and smaller specimens. Yet, staining remains a very active area of development, with methodological improvements occurring across multiple disciplines. For example, the gadolinium staining trialled here (Fig. 4E) has not previously been used in the field of reproductive anatomy, and instead was developed for staining brains in neuroscience (Kim et al. 2009; Ullmann et al. 2010). Imaging innovations developed on other soft tissue structures will undoubtedly be brought to bear on reproductive structures in the future.

Achieving the desired resolutions from MRI and CT imaging remains a perennial challenge when imaging delicate soft tissues. Despite the improved resolution of micro CT relative to medical CT, which we show-case here at 21 μm (Fig. 1E). Even higher resolutions of 0.2 µm can be achieved using a sub-micron CT scan-ner, such as the Zeiss Versa 520, which we used in our case study achieving 17 μm (Fig. 2A). The application of multiscalar imaging to female reproductive tissues could also prove particularly beneficial in addressing the problem of resolution. Applying a suite of imaging tools, such as medical CT, micro CT, sub-micron CT, and histology, that can span a hierarchy of tissue organizational levels of a given study animal will offer an unprecedented level of anatomical detail. Advances in automatic alignment and co-registration of image data from multiple modalities can improve the identification and segmentation of small features that may otherwise prove challenging to extract. Such an approach has been applied to skeletal elements (Museyko et al. 2015), brain tissues (Khimchenko et al. 2016), and respiratory tissues (Lawson et al. 2021), but has yet to be used on reproductive organs.

In addition to the practicalities of scanning itself, the processing of extracting 3D metrics from 2D tomographic data is still both challenging and time-consuming, and often relies on manual segmentation of structures that are not easily discernible. For example, in our case study there were several elements that needed manual segmentation as opposed to automatic or threshold segmentation by the software, most likely due to the reduced variation in contrast. The vast majority of the models created during this case study were manually segmented, with the only computer-assisted segmentation conducted on the bone structures of CT scanned, unstained specimens (see Figs. 1C, 3C, and D). The unstained specimen used to evaluate silicone casting in Fig. 3(B) provides a visual example of the fine differences between gray-scale values that enable threshold or manual segmentation. Here, the bones could be segmented using a threshold; however, the silicone rubber (arrow in Fig. 3B) could only be manually segmented. Efforts to improve image contrast are by far the most efficient means of reducing the burden of manual segmentation. Beyond this, machine learning tools have shown some promise in automating the segmentation of iodine contrast-enhanced CT of soft tissues (Mahmood et al. 2022) and are already well-established in the field of MRI (Akkus et al. 2017). The human uterus has been segmented from MRI using neural networks (Kurata et al. 2019), as have human cervical tumors (Hua et al. 2020), but this technology is yet to be broadly applied outside a clinical setting.

As well as the practical challenges associated with imaging the female reproductive system, there is a fundamental research limitation in solely considering the female reproductive system in isolation of the male. A newly developed technique to assess anatomical fit during copulation has been carried out on a variety of species (cetaceans and pinniped, Orbach et al. 2017b; alligator, Moore et al. 2021). These methods involve inflation of the male erectile tissue, usually via pressurized saline, to simulate erection. The inflated phallus is then inserted into the frozen-thawed reproductive tract of a female of the same species. Once alignment of the genitalia is determined the specimens are chemically fixed and CT scanned. This technique assesses how well the genitalia "fit" together during copulation, with the aim of potentially illuminating either congruent or antagonistic interactions and potential coevolution of male and female genitalia (Orbach et al. 2017b). Additional methods offer further progression from static considerations of morphology to the X-ray capture of moving data. X-ray Reconstruction of Moving Morphology (XROMM; Brainerd et al. 2010), is a 3D imaging workflow that utilizes bi-planar fluoroscopy to visualize skeletal movement *in vivo*. The male penis bone is a large and robust genital feature within several mammalian groups (Brassey et al. 2020), the nature of the size and thickness of this bone could offer the chance to visualize its movement during copulation via X-ray imaging, thus illuminating the inherently hidden mechanics of copulation in an internally fertilizing species. Examining the genitals of both sexes and how they interact may help address complex evolutionary questions regarding functional morphology.

Conclusions

The rise of 3D imaging techniques offers us novel insights into the female reproductive system, that have

never before been realized. Indeed, the amniote female reproductive system is challenging due to complicated internal morphology and large proportion of soft-tissue structures, making them an ideal testbed for trialling, validating, and developing imaging technology and associated image processing techniques. There are many improvements to be made in this area, especially in image contrast, resolution, scan times, standardization of techniques, and image processing to extract useful metrics. However, these technologies are constantly evolving within the field of imaging, drawing on techniques developed outside of reproductive anatomy, including medicine, neuroscience, biomechanics, and engineering. Applying new contrast agents, novel scanning technologies and the use of Artificial Intelligence to improve segmentation algorithms will all improve the imaging of female reproductive anatomy in the future. The potential for further exploration of reproductive anatomy in female amniotes is abundant, with many of the techniques reviewed, herein, illustrating the capacity to analyze female genital structures on both a macro- and a micro-scale. Imaging techniques such as these can not only help to quantify typically challenging female internal structures but could also begin to address the rich evolutionary dynamics that might occur between the sexes, thus enhancing our understanding of the functional morphology and evolution of genitalia.

Funding

EC has a match-funded PhD studentship agreement between both Manchester Metropolitan University and Williamson Park Zoo, Lancaster City Council. CAB was funded by a BBSRC Future Leader Fellowship grant BB/N01957/2. This work was supported by the National Research Facility for Lab X-ray CT (NXCT) through EPSRC grant EP/T02593X/1 and the Centre for Preclinical Imaging, which is funded by the grants from the MRC as well as the Wellcome Trust—208389/Z/17/Z.

Acknowledgments

The authors would like to acknowledge the organizers of this symposium—Dr Patricia Brennan and Professor Gunter Wagner. We also thank Dr Andrew Kitchener and Georg Hankte (National Museums Scotland), as well as Dr Dave Parish (Game and Wildlife Conservation Trust) for providing the necessary specimens for data collection. We would also like to thank Dr Amin Garbout and Dr Elizabeth Evans (National X-ray Computed Tomography Facility, University of Manchester) along with Professor Harish Poptani and Dr Mark Platt (University of Liverpool) for their advice with staining protocols and help in collecting micro CT and MRI image data, respectively.

Supplementary data

Supplementary data available at *ICB* online.

Data availability statement

The data underlying this article are available via morphosource.org, project number 435879 (https://www.morphosource.org/projects/000435879).

References

Abdelrahman AS, Ibrahim AS, Hetta WM, Elbohoty AE, Guirguis MS. 2014. The role of multidetector CT virtual hysterosalpingography in the evaluation of female infertility. Egypt J Radiol Nuclear Med 45:959–67.

Adams DC, Rohlf FJ, Slice DE. 2004. Geometric morphometrics: ten years of progress following the 'revolution'. Ital J Zool 71:5–16.

Adkesson MJ. 2018. Use of computed tomography–guided percarapacial ovocentesis in the management of dystocia in an eastern box turtle (*Terrapene carolina*). J Zoo Wildl Med 49:1007–11.

Agut A, Carrillo JD, Anson A, Belda E, Soler M. 2016. Imaging diagnosis—urethrovaginal fistula caused by a migrating grass awn in the vagina. Vet Radiol Ultrasound 57:E30–3.

Ah-King M, Barron AB, Herberstein ME. 2014. Genital evolution: why are females still understudied?. PLoS Biol 12:e1001851.

Akkus Z, Galimzianova A, Hoogi A, Rubin DL, Erickson BJ. 2017. Deep learning for brain MRI segmentation: state of the art and future directions. J Digit Imag 30:449–59.

Ali A, Derar DR. 2020. Ovary and ovarian bursa in dromedary camels: clinical relevance of the topographical features. Anat Histol Embryol 49:325–32.

Allisy-Roberts PJ, Williams J. 2007. Farr's physics for medical imaging. Amsterdam: Elsevier Health Sciences.

Amstislavsky S, Ternovskaya Y 2000. Reproduction in mustelids. Anim Reprod Sci 60–61, 571–81.

Arai Y, Yamada A, Ninomiya T, Kato T, Masuda Y. 2005. Micro-computed tomography newly developed for in vivo small animal imaging. Oral Radiol 21:14–8.

Arslan MF, Haridis A, Rosin PL, Tari S, Brassey C, Gardiner JD, Genctav A, Genctav M. 2021. SHREC'21: quantifying shape complexity. Comput Grap 102 144–53.

Aungier SPM, Roche JF, Sheehy M, Crowe MA. 2012. Effects of management and health on the use of activity monitoring for estrus detection in dairy cows. J Dairy Sci 95:2452–66.

Avni R, Neeman M, Garbow JR. 2015. Functional MRI of the placenta–from rodents to humans. Placenta 36:615–22.

Aymen J, Lamglait B, Wong E, Carmel ÉN, Lair S, Maccolini É. 2020. Ovarian carcinoma with skeletal metastasis in a Yacare Caiman (*Caiman yacare*). J Herpetol Med Surg 30:123–8.

Bardua C, Felice RN, Watanabe A, Fabre AC, Goswami A. 2019. A practical guide to sliding and surface semilandmarks in morphometric analyses. Integr Organ Biol 1:obz016.

Barozzi MCM, Saba CF, Gendron KP. 2021. CT characteristics of uterine and vaginal mesenchymal tumours in dogs. J Small Anim Pract 62:293–9.
Beaupied H, Lespessailles E, Benhamou CL. 2007. Evaluation of macrostructural bone biomechanics. Joint Bone Spine 74: 233–9.
Behr SC, Courtier JL, Qayyum A. 2012. Imaging of müllerian duct anomalies. Radiographics 32:E233–50.
Berquist RM, Gledhill KM, Peterson MW, Doan AH, Baxter GT, Yopak KE, Kang N, Walker HJ, Hastings PA, Frank LR. 2012. The Digital Fish Library: using MRI to digitize, database, and document the morphological diversity of fish. PLoS ONE 7:e34499.
Bird ST, Gelperin K, Sahin L, Bleich KB, Fazio-Eynullayeva E, Woods C, Radden E, Greene P, McCloskey C, Johnson T et al. 2019. First-trimester exposure to gadolinium-based contrast agents: a utilization study of 4.6 million US pregnancies. Radiology 293:193–200.
Bitar R, Leung G, Perng R, Tadros S, Moody AR, Sarrazin J, McGregor C, Christakis M, Symons S, Nelson A et al. 2006. MR pulse sequences: what every radiologist wants to know but is afraid to ask. Radiographics 26:513–37.
Boerckel JD, Mason DE, McDermott AM, Alsberg E. 2014. Microcomputed tomography: approaches and applications in bioengineering. Stem Cell Res Ther 5:1–12.
Bookstein FL. 1978. The measurement of biological shape and shape change. In: Lecture notes in biomathematics. Vol 24. Switzerland: Springer Nature, p. 445.
Bookstein FL. 1997. Landmark methods for forms without landmarks: morphometrics of group differences in outline shape. Med Image Anal 1:225–43.
Boyer DM, Puente J, Gladman JT, Glynn C, Mukherjee S, Yapuncich GS, Daubechies I. 2015. A new fully automated approach for aligning and comparing shapes. Anat Rec 298:249–76.
Brainerd EL, Baier DB, Gatesy SM, Hedrick TL, Metzger KA, Gilbert SL, Crisco JJ. 2010. X-ray reconstruction of moving morphology (XROMM): precision, accuracy and applications in comparative biomechanics research. J Exp Zool Part A Ecol Genet Physiol 313:262–79.
Brassey CA, Behnsen J, Gardiner JD. 2020. Postcopulatory sexual selection and the evolution of shape complexity in the carnivoran baculum. Proc R Soc B Biol Sci 287:20201883.
Brassey CA, Gardiner JD, Kitchener AC. 2018. Testing hypotheses for the function of the carnivoran baculum using finite-element analysis. Proc R Soc B Biol Sci 285:20181473.
Brennan PL, Sterett M, DiBuono M, Lara Granados G, Klo K, Marsden R, Schleinig P, Tanner L, Purdy S. 2021. Intrahorn penile intromission in the Alpaca *Vicugna pacos* and consequences to genital morphology. Integr Comp Biol 61: 624–33.
Butler R, Fernandez V, Nesbitt SJ, Leite JV, Gower D. 2022. A new pseudosuchian archosaur, *Mambawakale ruhuhu* gen. et sp. nov., from the Middle Triassic Manda Beds of Tanzania. R Soc Open Sci 9:211622.
Callahan S, Crowe-Riddell JM, Nagesan RS, Gray JA, Davis Rabosky AR. 2021. A guide for optimal iodine staining and high-throughput diceCT scanning in snakes. Ecol Evol 11:11587–603.
Campbell GM, Sophocleous A. 2014. Quantitative analysis of bone and soft tissue by micro-computed tomography: applications to ex vivo and in vivo studies. BoneKEy Rep 3:564
Carr MW, Grey ML. 2002. Magnetic resonance imaging: overview, risks, and safety measures. Am J Nurs 102:26–33.
Cunningham JA, Rahman IA, Lautenschlager S, Rayfield EJ, Donoghue PC. 2014. A virtual world of paleontology. Trends Ecol Evol 29:347–57.
Cushing AC, Noonan B, Gutman MR, Pillai SP. 2013. Intrauterine fetal death with subsequent quill exfoliation and dissemination in a North American porcupine (*Erethizon dorsatum*). J Zoo Wildl Med 44:1102–6.
Czisch M, Coppack T, Berthold P, Auer DP. 2001. In vivo magnetic resonance imaging of the reproductive organs in a passerine bird species. J Avian Biol 32:278–81.
d'Ovidio D, Melidone R, Rossi G, Albarella S, Noviello E, Fioretti A, Meomartino L. 2015. Multiple congenital malformations in a ferret (*Mustela putorius furo*). J Exot Pet Med 24:92–7.
Danil K, Leger JAS, Dennison S, De Quirós YB, Scadeng M, Nilson E, Beaulieu N. 2014. *Clostridium perfringens* septicemia in a long-beaked common dolphin *Delphinus capensis*: an etiology of gas bubble accumulation in cetaceans. Dis Aquat Organ 111:183–90.
Davies TG, Rahman IA, Lautenschlager S, Cunningham JA, Asher RJ, Barrett PM, Donoghue PC. 2017. Open data and digital morphology. Proc R Soc B Biol Sci 284:20170194.
Dawood Y. , Hagoort J., Siadari B. A., Ruijter J. M., Gunst Q. D., Lobe N. H. J., Strijkers G. J., de Bakker B. S., van den Hoff M. J. B. 2021. Reducing soft-tissue shrinkage artefacts caused by staining with Lugol's solution. Scientific reports 11:1–12.
Dayan MO, Besoluk K. 2011. Three-dimensional reconstruction from computed tomography images of respiratory system in New Zealand rabbits. Eurasian J Vet Sci 27:145–8.
Descamps E, Sochacka A, De Kegel B, Van Loo D, Van Hoorebeke L, Adriaens D. 2014. Soft tissue discrimination with contrast agents using micro-CT scanning. Belgian J Zool 144:20–40.
Di Ianni F, Volta A, Pelizzone I, Manfredi S, Gnudi G, Parmigiani E. 2015. Diagnostic sensitivity of ultrasound, radiography and computed tomography for gender determination in four species of lizards. Vet Radiol Ultrasound 56:40–5.
Doost A, Rangel A, Nguyen Q, Morahan G, Arnolda L. 2020. Micro-CT scan with virtual dissection of left ventricle is a non-destructive, reproducible alternative to dissection and weighing for left ventricular size. Sci Rep 10:1–9.
Dragonfly. 2021. 2021.1.0.977 [Computer software]. Montreal: Object Research Systems (ORS) Inc. http://www.theobjects.com/dragonfly [Accessed February 2022].
Du Plessis A, Broeckhoven C, Guelpa A, Le Roux SG. 2017. Laboratory x-ray micro-computed tomography: a user guideline for biological samples. Gigascience 6:gix027.
Du Y, Fan TY, Tan Y, Xiong Z, Wang Z. 2010. Seasonal changes in the reproductive physiology of female rhesus macaques (*Macaca mulatta*). J Am Assoc Lab Anim Sci 49:289–93.
Eberhard WG. 2010. Evolution of genitalia: theories, evidence, and new directions. Genetica 138:5–18.
Edelman RR, Koktzoglou I. 2019. Noncontrast MR angiography: an update. J Magn Reson Imag 49:355–73.
England GC, Allen WE. 1989. Real-time ultrasonic imaging of the ovary and uterus of the dog. J Reproduct Ferti Suppl 39:91–100.
Erlacher-Reid CD, Norton TM, Harms CA, Thompson R, Reese DJ, Walsh MT, Stamper MA. 2013. Intestinal and cloacal strictures in free-ranging and aquarium-maintained green sea turtles (*Chelonia mydas*). J Zoo Wildl Med 44:408–29.

Feldkamp LA, Goldstein SA, Parfitt MA, Jesion G, Kleerekoper M. 1989. The direct examination of three-dimensional bone architecture in vitro by computed tomography. J Bone Miner Res 4:3–11.

Fleckenstein JL, Archer BT, Barker BA, Vaughan JT, Parkey RW, Peshock RM. 1991. Fast short-tau inversion-recovery MR imaging. Radiology 179:499–504.

Flouri D, Darby JR, Holman SL, Perumal SR, David AL, Morrison JL, Melbourne A. 2021. Magnetic resonance imaging of placentome development in the pregnant Ewe. Placenta 105:61–9.

Fredieu JR, Kerbo J, Herron M, Klatte R, Cooke M. 2015. Anatomical models: a digital revolution. Med Sci Educ 25:183–94.

Garcia A, Van Der Weijden GC, Colenbrander B, Bevers MM. 1999. Monitoring follicular development in cattle by real-time ultrasonography: a review. Vet Rec 145:334–40.

Garland MR, Lawler LP, Whitaker BR, Walker ID, Corl FM, Fishman EK. 2002. Modern CT applications in veterinary medicine. Radiographics 22:55–62.

Gartrell BD, Girling JE, Edwards A, Jones SM. 2002. Comparison of noninvasive methods for the evaluation of female reproductive condition in a large viviparous lizard, *Tiliqua nigrolute*a. Zoo Biol 21:253–68.

Gavin PR. 2011. Growth of clinical veterinary magnetic resonance imaging. Vet Radiol Ultrasound 52:S2–4.

Geva T. 2006. Magnetic resonance imaging: historical perspective. J Cardiovasc Magn Reson 8:573–80.

Gignac PM, Kley NJ, Clarke JA, Colbert MW, Morhardt AC, Cerio D, Cost IN, Cox PG, Daza JD, Early CM et al. 2016. Diffusible iodine-based contrast-enhanced computed tomography (diceCT): an emerging tool for rapid, high-resolution, 3-D imaging of metazoan soft tissues. J Anat 228:889–909.

Gignac PM, Kley NJ. 2014. Iodine-enhanced micro-CT imaging: methodological refinements for the study of the soft-tissue anatomy of post-embryonic vertebrates. J Exp Zool Part B Mol Dev Evol 322:166–76.

Gignac PM, Kley NJ. 2018. The utility of diceCT imaging for high-throughput comparative neuroanatomical studies. Brain Behav Evol 91:180–90.

Gillenwater SJ. 2017. Novel approach to optimize the Laying Hen Model of ovarian cancer [Doctoral dissertation]. [College Station (TX)]: Texas A&M University.

Glaw F, Köhler J, Hawlitschek O, Ratsoavina FM, Rakotoarison A, Scherz MD, Vences M. 2021. Extreme miniaturization of a new amniote vertebrate and insights into the evolution of genital size in chameleons. Sci Rep 11:1–14.

Golding SJ, Shrimpton PC. 2002. Radiation dose in CT: are we meeting the challenge?. Br J Radiol 75;1–4.

Goldman LW. 2008. Principles of CT: multislice CT. J Nucl Med Technol 36:57–68.

Gumpenberger M, Henninger W. 2001. The use of computed tomography in avian and reptile medicine. In: Seminars in avian and exotic Pet Medicine. Vol. 4. London: WB Saunders. p. 174–80

Gumpenberger M. 2017. Diagnostic imaging of reproductive tract disorders in reptiles. Vet Clin Exot Anim Pract 20:327–43.

Hagen CK, Endrizzi M, Towns R, Meganck JA, Olivo A. 2020. A preliminary investigation into the use of edge illumination X-ray phase contrast micro-CT for preclinical imaging. Mol Imaging Biol 22:539–48.

Hayashi A, Tanaka H, Tajima T, Nakayama M, Ohashi F. 2013. A spayed female cat with squamous cell carcinoma in the uterine remnant. J Vet Med Sci 75:391–3.

Hedrick B. P., Antalek-Schrag, P., Conith A. J., Natanson L. J., Brennan P. L. 2019. Variability and asymmetry in the shape of the spiny dogfish vagina revealed by 2D and 3D geometric morphometrics.. Journal of Zoology 308:16–27.

Hounsfield GN. 1973. Computerized transverse axial scanning (tomography): part 1. Description of system. Br J Radiol 46:1016–22.

Hsieh J, Londt J, Vass M, Li J, Tang X, Okerlund D. 2006. Step-and-shoot data acquisition and reconstruction for cardiac x-ray computed tomography. Med Phys 33:4236–48.

Hsieh J. 2000. Tomographic reconstruction for tilted helical multislice CT. IEEE Trans Med Imag 19:864–72.

Hua W, Xiao T, Jiang X, Liu Z, Wang M, Zheng H, Wang S. 2020. Lymph-vascular space invasion prediction in cervical cancer: exploring radiomics and deep learning multilevel features of tumor and peritumor tissue on multiparametric MRI. Biomed Signal Process Control 58:101869.

Ibrahim MA, Hazhirkarzar B, Dublin AB. 2018. Gadolinium magnetic resonance imaging. In: StatPearls. Treasure Island (FL): StatPearls Publishing. [Updated 2021 July 9]. .

Kagadis GC, Loudos G, Katsanos K, Langer SG, Nikiforidis GC. 2010. In vivo small animal imaging: current status and future prospects. Med Phys 37:6421–42.

Kasban H, El-Bendary MAM, Salama DH. 2015. A comparative study of medical imaging techniques. Int J Inf Sci Intell Syst 4:37–58.

Kelly DA. 2016. Intromittent organ morphology and biomechanics: defining the physical challenges of copulation. Integr Comp Biol 56:705–14.

Khimchenko A, Deyhle H, Schulz G, Schweighauser G, Hench J, Chicherova N, Bikis C, Hieber SE, Müller B. 2016. Extending two-dimensional histology into the third dimension through conventional micro computed tomography. Neuroimage 139:26–36.

Kim S, Pickup S, Hsu O, Poptani H. 2009. Enhanced delineation of white matter structures of the fixed mouse brain using Gd-DTPA in microscopic MRI. NMR Biomed 22: 303–9.

Kinkel K, Frei KA, Balleyguier C, Chapron C. 2006. Diagnosis of endometriosis with imaging: a review. Eur Radiol 16: 285–98.

Kinoshita T, Yamakawa K, Matsuda H, Yoshikawa Y, Wada D, Hamasaki T, Fujimi S. 2019. The survival benefit of a novel trauma workflow that includes immediate whole-body computed tomography, surgery, and interventional radiology, all in one trauma resuscitation room: a retrospective historical control study. Ann Surg 269, 370.

Konicek C, Pees M, Gumpenberger M. 2020. Reproductive tract diseases in female backyard chickens (*Gallus gallus domesticus*)–diagnostic imaging and final outcome during a decade. Tierärztliche Praxis Ausgabe K: Kleintiere/Heimtiere 48:99–110.

Kummrow MS, Smith DA, Crawshaw G, Mastromonaco GF. 2010. Characterization of fecal hormone patterns associated with the reproductive cycle in female veiled chameleons (*Chamaeleo calyptratus*). Gen Comp Endocrinol 168:340–8.

Kurata Y, Nishio M, Kido A, Fujimoto K, Yakami M, Isoda H, Togashi K. 2019. Automatic segmentation of the uterus on

MRI using a convolutional neural network. Comput Biol Med 114:103438.
Lamb JC, IV, Newbold RR, Stumpf WE, McLachlan JA. 1978. Transitional changes in the surface epithelium of the cycling mouse vagina, cervix and uterus: scanning electron microscopic studies. Biol Reprod 19:701–11.
Lauridsen H, Hansen K, Wang T, Agger P, Andersen JL, Knudsen PS, Rasmussen AS, Uhrenholt L, Pedersen M. 2011. Inside out: modern imaging techniques to reveal animal anatomy. PLoS ONE 6:e17879.
Lawson MJ, Katsamenis OL, Chatelet D, Alzetani A, Larkin O, Haig I, Lackie P, Warner J, Schneider P. 2021. Immunofluorescence-guided segmentation of three-dimensional features in micro-computed tomography datasets of human lung tissue. R Soc Open Sci 8:211067.
Lazaridis LJ, Brozos CN, Kissis E. 2012. Applications of ultrasonography in ruminants (II): female reproductive system-a review. J Hellenic Vet Med Soc 63:74–88.
Lee Jr FT, Grist TM, Nelson KG, Chosy SG, Rappe AH, Shapiro SS, Kelcz F. 1996. MR hysterosalpingography in a rabbit model. J Magn Reson Imaging 6:300–4.
Lemma A. 2013. The role of trans-rectal ultrasonography in artificial insemination program. In: Success in artificial insemination-quality of semen and diagnostics employed. London: IntechOpen.
Lindeberg H. 2008. Reproduction of the female ferret (*Mustela putorius furo*). Reproduct Domest Anim 43:150–6.
Mahmood U. , Bates D. D., Erdi Y. E., Mannelli L., Corrias G., Kanan C 2022. Deep Learning and Domain-Specific Knowledge to Segment the Liver from Synthetic Dual Energy CT Iodine Scans. Diagnostics 12:672.
Mannelli L, Maki JH, Osman SF, Chandarana H, Lomas DJ, Shuman WP, Linnau KF, Green DE, Laffi G, Moshiri M. 2012. Noncontrast functional MRI of the kidneys. Curr Urol Rep 13:99–107.
Mayor P, Guimarães DA, López C. 2013. Functional morphology of the genital organs in the wild paca (*Cuniculus paca*) female. Anim Reprod Sci 140:206–15.
McNanley AR, Johnson AM, Flynn MK, Wood RW, Kennedy SD, Reeder JE. 2009. Inherited pelvic organ prolapse in the mouse: preliminary evaluation of a new murine model. Int Urogynecol J 20:19–25.
Metscher BD. 2009. MicroCT for comparative morphology: simple staining methods allow high-contrast 3D imaging of diverse non-mineralized animal tissues. BMC Physiol 9: 1–14.
Metscher BD. 2011. X-ray microtomographic imaging of intact vertebrate embryos. Cold Spring Harb Protoc 2011:pdb–prot067033.
Mitteroecker P. 2020. Morphometrics in evolutionary developmental biology. Evol Dev Biol 40: 941–51.
Mizutani R, Suzuki Y. 2012. X-ray microtomography in biology. Micron 43:104–15.
Moore BC, Brennan PL, Francis R, Penland S, Shiavone K, Wayne K, Woodward AR, Does MD, Kim DK, Kelly DA. 2021. Glans inflation morphology and female cloaca copulatory interactions of the male American alligator phallus. Biol Reprod 104:374–86.
Moser E, Stadlbauer A, Windischberger C, Quick HH, Ladd ME. 2009. Magnetic resonance imaging methodology. Eur J Nucl Med Mol Imaging 36:30–41.
Museyko O, Marshall RP, Lu J, Hess A, Schett G, Amling M, Kalender WA, Engelke K. 2015. Registration of 2D histological sections with 3D micro-CT datasets from small animal vertebrae and tibiae. Comput Meth Biomech Biomed Eng 18:1658–73.
Orbach DN, Brennan PL, Hedrick BP, Keener W, Webber MA, Mesnick SL. 2020. Asymmetric and spiraled genitalia coevolve with unique lateralized mating behavior. Sci Rep 10:1–8.
Orbach DN, Kelly DA, Solano M, Brennan PL. 2017b. Genital interactions during simulated copulation among marine mammals. Proc R Soc B Biol Sci 284:20171265.
Orbach DN, Marshall CD, Mesnick SL, Würsig B. 2017a. Patterns of cetacean vaginal folds yield insights into functionality. PLoS ONE 12:e0175037.
Orbach DN, Marshall CD, Würsig B, Mesnick SL. 2016. Variation in female reproductive tract morphology of the common bottlenose dolphin (*Tursiops truncatus*). Anat Rec 299:520–37.
oVert. 2017. Digitization TCN: collaborative research: oVert: open exploration of vertebrate diversity in 3D. https://www.nsf.gov/awardsearch/showAward?AWD_ID=1701714; https://www.floridamuseum.ufl.edu/science/overt/ [Accessed April 2022].
Palmer BD, Guillette LJ, Jr. 1988. Histology and functional morphology of the female reproductive tract of the tortoise *Gopherus polyphemus*. Am J Anat 183:200–11.
Pauwels E, Van Loo D, Cornillie P, Brabant L, Van Hoorebeke L. 2013. An exploratory study of contrast agents for soft tissue visualization by means of high resolution X-ray computed tomography imaging. J Microsc 250:21–31.
Pecile A, Groppetti D, Grieco V, Barella G, Moioli M, Faverzani S. 2017. Asymptomatic unilateral ovarian leiomyoma in a German Shepherd bitch. Macedon Vet Rev 40:97–101.
Perkins MJ, Palmer BD. 1996. Histology and functional morphology of the oviduct of an oviparous snake, *Diadophis punctatus*. J Morphol 227:67–79.
Pinkernelle JG, Stelter L, Hamm B, Teichgräber U. 2008. Small animal MRI: clinical MRI as an interface to basic biomedical research. Rofo: Fortschritte auf dem Gebiete der Rontgenstrahlen und der Nuklearmedizin 180:505–13.
Psychoyos A, Mandon P. 1971. Scanning electron microscopy of the surface of the rat uterine epithelium during delayed implantation. Reproduction 26:137–NP.
Racicot R. 2021. Evolution of whale sensory ecology: frontiers in nondestructive anatomical investigations. Anat Rec 350: 237584675.
Ramsay EC, Tytle T, Carey JC, Tytle R. 1985. Hysterosalpingography in gorilla. J Zoo Anim Med 16:85–9.
Reichardt M, Töpperwien M, Khan A, Alves F, Salditt T. 2020. Fiber orientation in a whole mouse heart reconstructed by laboratory phase-contrast micro-CT. J Med Imag 7:1.
Ross CF, Iriarte-Diaz J, Nunn CL. 2012. Innovative approaches to the relationship between diet and mandibular morphology in primates. Int J Primatol 33:632–60.
Rowan C, Cuddy L, Bryan J, Shiel R, Hoey S. 2017. Imaging diagnosis—computed tomography findings in a case of metastatic ovarian adenocarcinoma in a dog. Vet Radiol Ultrasound 58:E60–3.
Rumery RE, Eddy EM. 1974. Scanning electron microscopy of the fimbriae and ampullae of rabbit oviducts. Anat Rec 178:83–101.

Samii VF, McLoughlin MA, Mattoon JS, Drost WT, Chew DJ, DiBartola SP, Hoshaw-Woodard S. 2004. Digital fluoroscopic excretory urography, digital fluoroscopic urethrography, helical computed tomography, and cystoscopy in 24 dogs with suspected ureteral ectopia. J Vet Intern Med 18: 271–81.

Santana SE. 2018. Comparative anatomy of bat jaw musculature via diffusible iodine-based contrast-enhanced computed tomography. Anat Rec 301:267–78.

Schambach SJ, Bag S, Schilling L, Groden C, Brockmann MA. 2010. Application of micro-CT in small animal imaging. Methods 50:2–13.

Shatil AS, Matsuda KM, Figley CR. 2016. A method for whole brain ex vivo magnetic resonance imaging with minimal susceptibility artifacts. Front Neurol 7:208.

Shen L, Farid H, McPeek MA. 2009. Modeling three-dimensional morphological structures using spherical harmonics. Evolution 63:1003–16.

Shen W, Chen J, Gantz M, Velasquez G, Punyanitya M, Heymsfield SB. 2012. A single MRI slice does not accurately predict visceral and subcutaneous adipose tissue changes during weight loss. Obesity 20:2458–63.

Sloan NS, Simmons LW. 2019. The evolution of female genitalia. J Evol Biol 32:882–99.

Sontas BH, Milani C, Romagnoli S, Bertolini G, Caldin M, Caliari D, Zappulli V, Mollo A. 2011. A huge ovarian cyst in a hysterectomized bitch. Reproduct Domest Anim 46: 1107–11.

Stolzenburg JU, Neuhaus J, Liatsikos EN, Schwalenberg T, Ludewig E, Ganzer R. 2006. Histomorphology of canine urethral sphincter systems, including three-dimensional reconstruction and magnetic resonance imaging. Urology 67:624–30.

Straub J, Jurina K. 2001. Magnetic resonance imaging in chelonians. In: Seminars in avian and exotic pet medicine. Vol. 4. London: WB Saunders. p. 181–6.

Sundaram M, McLeod RA. 1990. MR imaging of tumor and tumorlike lesions of bone and soft tissue. Am J Roentgenol 155, 817–24.

Sutton M, Rahman I. Garwood R 2013. Techniques for virtual palaeontology. Hoboken (NJ): John Wiley & Sons.

Tao S, He C, Hao X, Kuang C, Liu X. 2021. Principles of different x-ray phase-contrast imaging: a review. Appl Sci 11: 2971.

Tsai HP, Turner ML, Manafzadeh AR, Gatesy SM. 2020. Contrast-enhanced XROMM reveals in vivo soft tissue interactions in the hip of *Alligator mississippiensis*. J Anat 236:288–304.

Tschopp P, Sherratt E, Sanger TJ, Groner AC, Aspiras AC, Hu JK, Pourquié O, Gros J, Tabin CJ. 2014. A relative shift in cloacal location repositions external genitalia in amniote evolution. Nature 516:391–4.

Tsuboi M, Kopperud BT, Syrowatka C, Grabowski M, Voje KL, Pélabon C, Hansen TF. 2020. Measuring complex morphological traits with 3D photogrammetry: a case study with deer antlers. Evol Biol 47:175–86.

Ullmann JF, Cowin G, Kurniawan ND, Collin SP. 2010. Magnetic resonance histology of the adult zebrafish brain: optimization of fixation and gadolinium contrast enhancement. NMR Biomed Int J Devot Dev Appl Magnet Resonance In vivo 23:341–6.

Valente ALS, Cuenca R, Zamora M, Parga ML, Lavin S, Alegre F, Marco I. 2007. Computed tomography of the vertebral column and coelomic structures in the normal loggerhead sea turtle (*Caretta caretta*). Vet J 174:362–70.

Valentin L. 2006. Imaging in gynecology. Best Pract Res Clin Obstetr Gynaecol 20:881–906.

Van Eijnatten M, van Dijk R, Dobbe J, Streekstra G, Koivisto J, Wolff J. 2018. CT image segmentation methods for bone used in medical additive manufacturing. Med Eng Phys 51: 6–16.

Veladiano IA, Banzato T, Bellini L, Montani A, Catania S, Zotti A. 2016. Normal computed tomographic features and reference values for the coelomic cavity in pet parrots. BMC Vet Res 12:1–9.

Verstraete KL, Lang P. 2000. Bone and soft tissue tumors: the role of contrast agents for MR imaging. Eur J Radiol 34:229–46.

Vischer N. 2013. PeakFinder Tool. http://simon.bio.uva.nl/objectj/examples/PeakFinder/peakfinder.html [Accessed January 2022].

Waberski D, Kunz-Schmidt A, Borchardt Neto G, Richter L, Weitze KF. 1999. Real-time ultrasound diagnosis of ovulation and ovarian cysts in sows and its impact on artificial insemination efficiency. J Anim Sci 77: 1–8. Proceedings of the American Society of Animal Science

Wahid MR, Prawira AY, Nisa' C, Agungpriyono S, Fakhrul Ulum M. 2020. Sonoanatomy of female reproductive organ of Sunda porcupine (*Hystrix javanica*). Anat Histol Embryol 49: 779–87.

Wang KY, Samii VF, Chew DJ, McLoughlin MA, DiBartola SP, Masty J, Lehman AM. 2006. Vestibular, vaginal and urethral relationships in spayed and intact normal dogs. Theriogenology 66:726–35.

Weiss DA, Rodriguez E, Jr, Cunha T, Menshenina J, Barcellos D, Chan LY, Cunha G. 2012. Morphology of the external genitalia of the adult male and female mice as an endpoint of sex differentiation. Mol Cell Endocrinol 354:94–102.

Weissman A, Jiménez D, Torres B, Cornell K, Holmes SP. 2013. Canine vaginal leiomyoma diagnosed by CT vaginourethrography. J Am Anim Hosp Assoc 49:394–7.

Wells PN. 1999. Ultrasonic imaging of the human body. Rep Prog Phys 62:671.

Wenzlow N, Tivers MS, Selmic LE, Scurrell EJ, Baines SJ, Smith KC. 2009. Haemangiosarcoma in the uterine remnant of a spayed female dog. J Small Anim Pract 50:488–91.

Wiczyk HP, Janus CL, Richards CJ, Graf MJ, Gendal ES, Rabinowitz JG, Laufer N. 1988. Comparison of magnetic resonance imaging and ultrasound in evaluating follicular and endometrial development throughout the normal cycle. Fertil Steril 49:969–72.

Willekens I, Buls N, Lahoutte T, Baeyens L, Vanhove C, Caveliers V, Deklerck R, Bossuyt A, De Mey J. 2010. Evaluation of the radiation dose in micro-CT with optimization of the scan protocol. Contrast Media Mol Imag 5:201–7.

Williams EJ, Fischer DP, Pfeiffer DU, England GC, Noakes DE, Dobson H, Sheldon IM. 2005. Clinical evaluation of postpartum vaginal mucus reflects uterine bacterial infection and the immune response in cattle. Theriogenology 63: 102–17.

Wojcieszek JM, Austin P, Harvey MS, Simmons LW. 2012. Micro-CT scanning provides insight into the functional morphology of millipede genitalia. J Zool 287:91–5.

Xiao YD, Paudel R, Liu J, Ma C, Zhang ZS, Zhou SK. 2016. MRI contrast agents: classification and application. Int J Mol Med 38:1319–26.

Ypsilantis P, Souftas V, Vyza V, Vraila M, Chatzaki M, Ypsilantou I, Pitiakoudis M. 2021. Magnetic resonance imaging for early pregnancy diagnosis in the laboratory rat. Lab Anim 55: 262–9.

Yu L, Liu X, Leng S, Kofler JM, Ramirez-Giraldo JC, Qu M, Christner J, Fletcher JG, McCollough CH. 2009. Radiation dose reduction in computed tomography: techniques and future perspective. Imag Med 1:65.

Zarb F, McNulty J, Gatt A, Formosa C, Chockalingam N, Evanoff MG, Rainford L. 2017. Comparison of in vivo vs. frozen vs. Thiel cadaver specimens in visualisation of anatomical structures of the ankle on proton density Magnetic Resonance Imaging (MRI) through a visual grading analysis (VGA) study. Radiography 23:117–24.

Ziegler A, Kunth M, Mueller S, Bock C, Pohmann R, Schröder L, Faber C, Giribet G. 2011. Application of magnetic resonance imaging in zoology. Zoomorphology 130:227–54.

Ziegler A, Mueller S. 2011. Analysis of freshly fixed and museum invertebrate specimens using high-resolution, high-throughput MRI. In: In vivo NMR Imaging. Totowa (NJ): Humana Press. p. 633–51.

Ziegler A, Ogurreck M, Steinke T, Beckmann F, Prohaska S, Ziegler A. 2010. Opportunities and challenges for digital morphology. Biol Direct 5:1–9.

Ziehmer B, Ogle S, Signorella A, Knorr C, Macdonald AA. 2010. Anatomy and histology of the reproductive tract of the female Babirusa (*Babyrousa celebensis*). Theriogenology 74:184–93.